Nucleation of spiral wave patterns at surface defects

Han Wei and G. Lilienkamp
Institut für Physik und Physikalische Technologien, Technische Universität Clausthal, Leibnizstr. 4, 38678 Clausthal-Zellerfeld, Germany

Jörn Davidsen
Max-Planck-Institut für Physik komplexer Systeme, Nöthnitzer Strasse 38, 01187 Dresden, Germany

Markus Bär
Fachbereich Mathematische Modellierung und Datenanalyse, Physikalisch-Technische Bundesanstalt, Abbestraße 2-12, 10587 Berlin, Germany

Ronald Imbihl
Institut für Physikalische Chemie und Elektrochemie, Universität Hannover, Callinstraße 3-3a, 30167 Hannover, Germany
(Received 18 September 2004; revised manuscript received 18 April 2005; published 12 January 2006)

The nucleation of spiral waves at a surface defect during catalytic CO oxidation on Pt(110) has been studied with a low energy electron microscope system. It is found that reaction fronts originate from a boundary layer between the defect and the surrounding Pt(110) area. The findings are corroborated by numerical simulations within a realistic reaction-diffusion model of the surface reaction.

DOI: 10.1103/PhysRevE.73.016210 PACS number(s): 45.70.Qj, 82.40.Np, 82.20.−w, 82.65.+r

Rotating spiral waves are frequently observed in reaction-diffusion (RD) systems including the well-known Belousov-Zhabotinskii (BZ) [1,2] reaction, aggregation of slime molds [3], catalytic CO oxidation [4–8], cardiac tissue [9], intracellular calcium dynamics in frog eggs [10], and glycolytic activity in extracts of yeast cells [11]. In some of these systems, rotating spiral waves appear to emerge spontaneously from an initially homogeneous spatial state. However, already the early experiments with the excitable BZ reaction demonstrated that a perturbation is required in an excitable system. This perturbation can either be provided by heterogeneous nucleation at an impurity or surface scratch or by external stimulation with a silver wire or laser beam. Elementary considerations yield the size of a critical nucleus [8,12]. Recently, the nucleus for formation of a double spiral has been stabilized in experiment and computed in a model using control techniques [13]. Little is known yet about the dynamics involved in the heterogeneous nucleation of spiral waves.

In this article we investigate the nucleation of spirals in catalytic CO oxidation on a Pt(110) surface by means of low energy electron microscopy (LEEM). Spirals are found to nucleate near large surface defects. The decisive role is played by a thin boundary layer around the defect which initiates all nucleation events. We illustrate events of successful and failed nucleation by experiments and numerical simulations with a realistic reaction-diffusion model of catalytic CO oxidation.

Catalytic CO oxidation proceeds via a Langmuir-Hinshelwood (LH) mechanism, that is, both molecules have to adsorb, CO as molecule and O_2 dissociatively, before they can react to form CO_2 which rapidly desorbs from the surface. A dense CO adlayer poisons the reaction and therefore two states exist in the kinetics—an inactive state where the surface is CO covered and an active state where the CO coverage is very low. Coupling the LH scheme to the CO-induced $1\times1 \rightleftharpoons 1\times2$ surface phase transition of Pt(110) makes the system excitable. Here, we study the reaction in a parameter range where the reaction is bistable but where both states are unstable with respect to a perturbation by diffusion [4,5,7]. As shown before, excitation of pulses and spiral waves is possible in this regime of "dynamic bistability" [7]. With our LEEM instrument we can obtain a resolution of about 150 Å [14,15] which is about one to two orders of magnitude better than that of the previous photoemission electron microscope (PEEM) studies of this system [4,5]. We chose an electron energy close to zero so that the instrument is operated at the boundary to mirror electron microscopy (MEM) [17]. Contrast in the MEM mode is based on work function differences as well as on surface topography. In the LEEM mode the reflectivity of the surface determines the contrast. The reaction is studied under low pressure conditions in the 10^{-5} mbar range and therefore practically isothermal.

The LEEM/MEM frame in Fig. 1(a) displays two surface defects imaged as dark areas and in the following we restrict ourselves to the larger one of the two defects. The smaller defect is also active but under different conditions. Under the specific energy chosen here the two stable states of the surface, CO covered and oxygen covered, are imaged as bright and dark areas, respectively [15]. The bright halo of approximately 30 μm diameter which asymmetrically surrounds the large defect is due to electrical charging, thus demonstrating that the "defect" is actually an electrically insulating impurity. Slight distortions in the shape of the defect seen in some of the images are due to this electrical charging and not caused by an actual size change. A plausible explanation consistent with the described facts is that the defect is a diamond particle which remained on the surface after polishing with diamond paste [16]. The diamond surface itself is

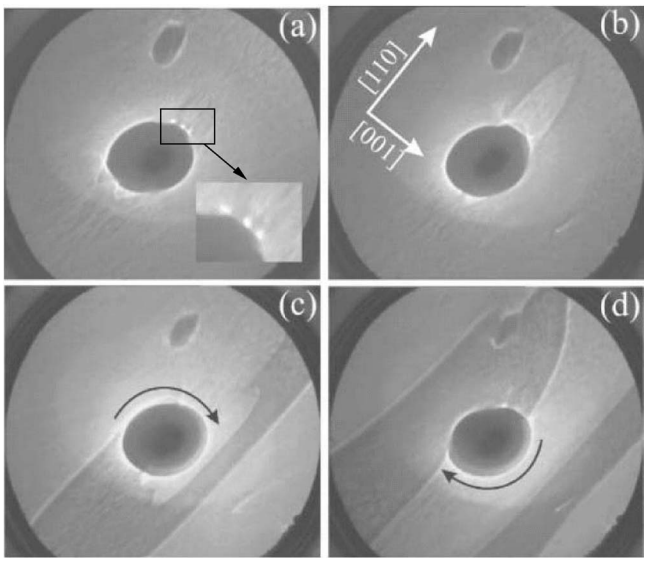

FIG. 1. Nucleation of a spiral wave at a surface defect. Experimental conditions: $T=402$ K, $p_{CO}>7\times10^{-6}$ mbar, $p_{O_2}=2\times10^{-5}$ mbar, $E=0$ eV. Field of view: 64×64 μm^2. (a) Two surface defects (dark) under conditions close to nucleation of a CO front. The inset shows the bound CO pulses on an enlarged scale. (b) Nucleation of a CO front at the defect in (a) ($t=0$ s). (c) and (d) Two stages in the rotation of a stable pinned spiral wave with a rotational period of 29.5 s.

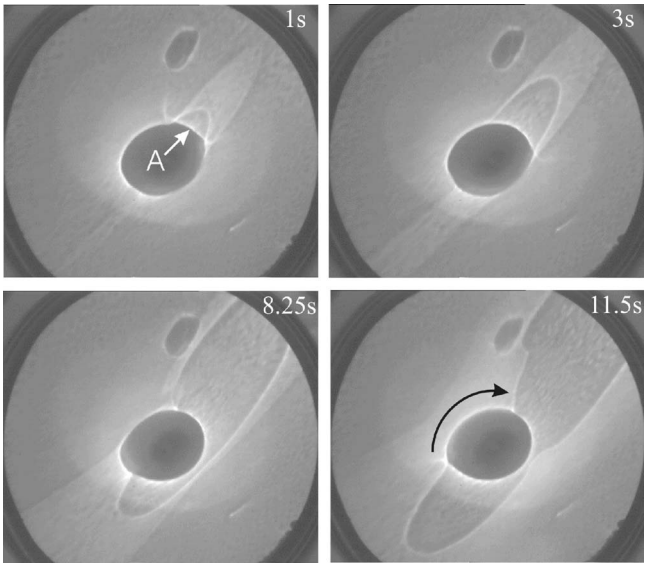

FIG. 2. Supercritical nucleation of a CO pulse at defect. The initial situation at $t=0$ s is given by Fig. 1(b), the final state by Figs. 1(c) and 1(d). At point *A* the CO front breaks and loses contact with the defect. Experimental conditions: $T=402$ K, $p_{CO}>7\times10^{-6}$ mbar, $p_{O_2}=2\times10^{-5}$ mbar, $E=0$ eV. Field of view: 64×64 μm^2.

practically inert but we can assume that mechanical stress exerted by the diamond particle has led to the strong structural distortion of the adjacent Pt layer or even made it amorphous, thus creating the boundary layer which shows up (Fig. 1) as bright ring of $1-2$ μm thickness surrounding the defect [18].

When we adjust p_{CO}/p_{O_2} conditions just below the threshold for ignition of a CO wave, we observe a bright boundary layer nearly completely surrounding the defect as shown in Fig. 1(a). We also note bright circular spots of $1-1.5$ μm diameter at the perimeter of the defect. These bright spots nucleate spontaneously at the boundary layer. They typically travel over only a short distance, merge with other bright spots or the bright part of the boundary layer, and, most importantly, they excite chemical waves in the surrounding medium. We can associate the traveling bright spots with bound CO pulses because they cannot leave the perimeter of the defect.

Upon a slight increase of p_{CO} one of the bound CO pulses ignites a CO front in the surrounding medium spreading out from the defect as shown in Fig. 1(b). The anisotropy of front propagation reflects the troughlike structure of the Pt(110) substrate with CO diffusion being fast along the [110]-oriented troughs and slow perpendicular to them [19]. Depending on whether such a nucleation leads to a stable spiral wave as shown in Figs. 1(c) and 1(d) or whether the excitation remains bound to the vicinity of the defect and soon dies away, we distinguish between a supercritical and a subcritical nucleation.

A supercritical nucleation is displayed in Fig. 2 showing the different stages in the development of the stable spiral wave displayed in Figs. 1(c) and 1(d). After nucleation of a CO front [Fig. 1(b)] an oxygen front nucleates inside the CO covered area at the 2 o'clock position (1 s). This front expands asymmetrically so that it reaches the left edge of the CO covered area earlier than the right edge (3 s). Simultaneously a CO front expands also on the bottom part of the defect and expands there rapidly (1 s and 3 s). The left upper part of the CO front now loses contact with the defect (8.25 s, *A*) while the oxygen front has advanced to the bottom of the defect forming an enlarging area (8.25 s and 11.5 s). A pulse rotating around the defect is created. In the following the CO covered area expands at the expense of the oxygen covered surface area so that at the end the stable oxygen spiral wave displayed in Figs. 1(c) and 1(d) results.

In order to transform a symmetrically growing CO front into a rotating spiral wave, symmetry breaking has to occur. The asymmetric growth of a front shown in Figs. 1 and 2 is one option but another possible mechanism is demonstrated in Fig. 3. After nucleation of a CO front (0 s) a bound CO pulse moves towards the front of the expanding CO area (not shown here). The collision of the CO front with the pulse consisting of a CO front and an oxygen back front annihilates the two CO fronts in the collision area (1.25 s). The oxygen back front combines with the remaining large CO front to a new pulse rotating clockwise around the defect. This pulse is not stable. The back front of the pulse advancing faster than the forefront catches up with the forefront so that the pulse is finally extinguished as shown in Fig. 3 (5 s and 11 s). In this last sequence, which we may call subcritical nucleation, p_{CO} has been slightly reduced compared to the supercritical nucleation displayed in Figs. 1 and 2.

The model of the catalytic CO oxidation on Pt(110) we study here is the simplified version introduced in Ref. [20]. It is similar to the well-known Barkley model [21] as well as to

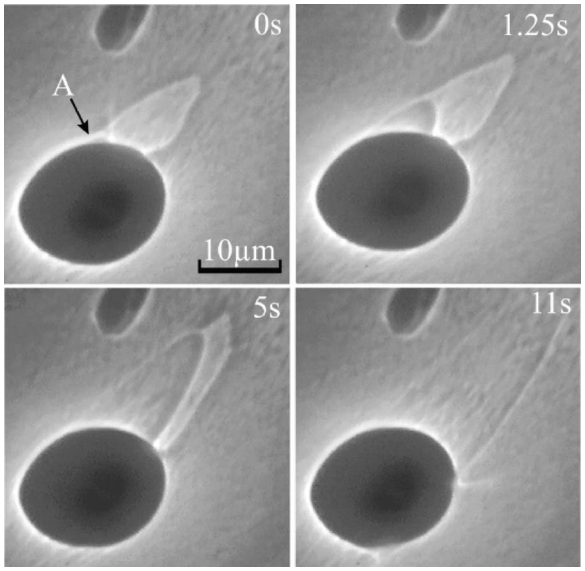

FIG. 3. Subcritical nucleation of a CO pulse at a defect. The point where the bound CO pulse and the CO front collided has been marked as *A*. Experimental conditions: $T=402$ K, $p_{CO}=7\times10^{-6}$ mbar, $p_{O_2}=2\times10^{-5}$ mbar, $E=0$ eV.

the FitzHugh-Nagumo equations which represent a standard model for excitable and bistable media [12]. This model of CO oxidation has been employed in the study of transitions from fronts to spirals under bistable conditions [7]. It is a two-component reaction-diffusion system in the bistable regime, describing the dynamics of the CO/O coverage u and the surface structure w. The equations read in dimensionless units

$$\frac{\partial u}{\partial t} = -\frac{1}{\epsilon}u(u-1)\left(u-\frac{b+w}{a}\right)+D_x\partial_x^2 u+D_y\partial_y^2 u,$$

$$\frac{\partial w}{\partial t} = f(u)-w,$$

$$f(u)=\begin{cases}0, & 0\leqslant u<0.6\\ 1-31.25(u-0.4)(u-1)^2, & 0.6\leqslant u\leqslant 1\\ 1, & 1<u.\end{cases} \quad (1)$$

Here, the special form of $f(u)$ is taken from the experimental dependence of the surface structure on the CO coverage. The quantity ϵ stands for the ratio of time scales of the surface reaction and surface restructuring, while a depends mostly on the surface temperature (assuming typical pressures in the range of 10^{-5} to 10^{-4} mbar). For a detailed discussion of the model, see Refs. [20,21]. Here we chose $\epsilon=0.025$ and $a=1.8$ throughout to take into account the observed bistability. The parameter b expresses whether CO or oxygen prevails on the surface; it becomes larger for increasing the partial CO pressure p_{CO}. D_x and D_y are the diffusion constant in x and y direction, respectively. Here, we chose $D_x=1$ and $D_y\leqslant D_x$. The experimentally observed anisotropy has generally a ratio of 4:1. Note that the anisotropy is neither sufficient nor crucial to yield spiral waves in the model.

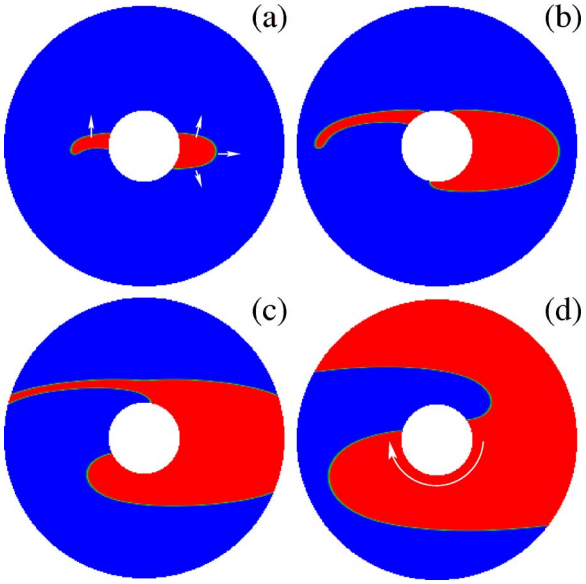

FIG. 4. (Color online) Simulation of the supercritical regime with boundary layer from an initial condition similar to the experimental situation in Fig. 3 at $t=3$ s. Red (blue) corresponds to $u=0$ ($u=1$) and a CO coverage of 0.95 (0.2) monolayers. The first three pictures show the initial dynamics of a CO pulse and CO front growing out of the boundary layer. Time between snapshots is 12 s. The last picture shows the system at a later state. Parameters are $D_y=0.25$, $b_{bulk}=0.425$.

To mimic the experimental situation, we consider a disk of diameter $L=128$ with no-flux boundary conditions [22]. The existence of a boundary layer favoring CO adsorption was described by setting the constant $b=0.46$ in a three-space-units-wide range around a defect of diameter $L_d=32$. The defect itself was assumed to be inert. First, we chose an initial condition comparable to the experiment in Fig. 3 at $t=3$ s; on the right side of the defect a CO front nucleates, while on the left side a pulselike CO patch is present (see Fig. 4). The collision of these objects reverses the upper part of the CO front and eventually gives rise to a spiral. The spiral in Fig. 4(d) is reminiscent of the experimentally observed spiral wave in Fig. 1(d).

Decreasing the parameter b (p_{CO}) leads eventually to the experimentally observed transition from the supercritical to the subcritical regime. In simulations without the boundary layer, the spiral starts to unpin from the defect below a threshold of $b_{cr,1}=0.406$ (see Fig. 5). Below a second critical value $b_{cr,2}=0.385$ pulses in one dimension become unstable via annihilation; compare this to Ref. [20]. Thus, the boundary layer stabilizes the pinning of the spiral to the defect and prevents the unpinning and retraction of the spiral.

Figure 6 shows a second important effect of the boundary layer. First, we have initiated a pulse in the boundary layer [similar to the experiment in Fig. 1(a)]. Then, the value of b in the bulk (corresponding to the partial CO pressure p_{CO}) is slowly increased. If we cross again $b_{cr,1}$, the pulse starts to proliferate a CO arm into the surroundings of the defect and finally a rotating spiral is seen (Fig. 6). This represents an alternative nucleation route which, of course, works only due to the presence of the boundary layer. So far, this behavior has not been seen in experiment.

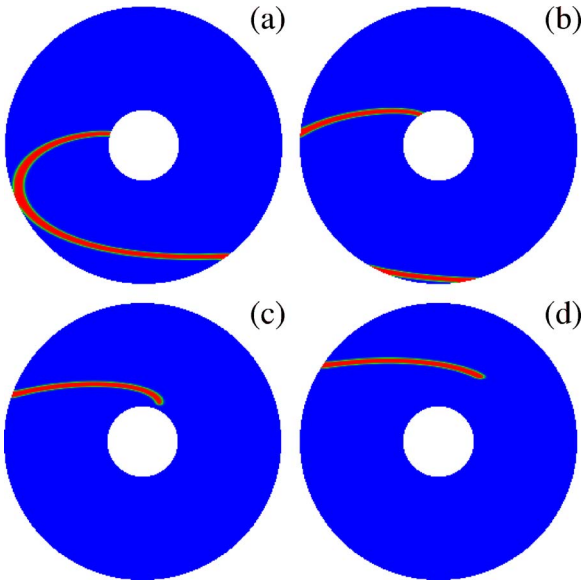

FIG. 5. (Color online) Simulation of the transition from super-to subcritical regime by reducing p_{CO} in the absence of a boundary layer. This leads to a detachment of the wave front from the defect. Color coding as in Fig. 4. Time between snapshots is 9 s and $D_y=1$, $b^{new}=0.406$, $b^{old}=0.407$.

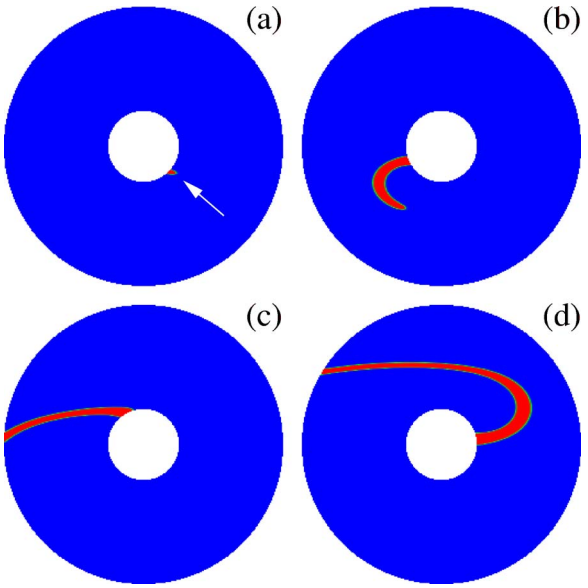

FIG. 6. (Color online) Simulation of the transition from sub-to supercritical regime by increasing p_{CO} with bound CO pulse (arrow) in the boundary layer. Color coding as in Fig. 4. Time between snapshots is 24 s and $D_y=0.25$, $b^{new}_{bulk}=0.425$, $b^{old}_{bulk}=0.38$.

In conclusion, we have shown that the dynamics in the boundary layer around a surface defect plays a crucial role in the nucleation of spiral waves. Depending on the control parameter, excitations either remain localized at the interface or they propagate into the surrounding area giving rise to the nucleation of fronts or pulses. Additional symmetry breaking by heterogeneities in the boundary layer or by collision with a bound CO pulse can transform an initially symmetrically growing CO front into a rotating spiral wave. Scenarios similar to those found here are expected in other catalytic reactions where impurities have modified the reactivity of their surroundings either through mechanical stress or through a chemical change.

Financial support from the German Israeli Science Foundation and the Deutsche Forschungsgemeinschaft is gratefully acknowledged.

[1] *Chemical Waves and Patterns*, edited by R. Kapral and K. Showalter (Kluwer, Dordrecht, 1994).
[2] A. T. Winfree, Science **175**, 634 (1972).
[3] G. Gerisch, Naturwiss. **58**, 430 (1971); P. Devreotes, Science **245**, 1045 (1989).
[4] S. Jakubith, H.-H. Rotermund, W. Engel, A. von Oertzen, and G. Ertl, Phys. Rev. Lett. **65**, 3013 (1990).
[5] S. Nettesheim, A. von Oertzen, H. H. Rotermund, and G. Ertl, J. Chem. Phys. **98**, 9977 (1993).
[6] R. Imbihl and G. Ertl, Chem. Rev. (Washington, D.C.) **95**, 697 (1995).
[7] M. Bär, S. Nettesheim, H. H. Rotermund, M. Eiswirth, and G. Ertl, Phys. Rev. Lett. **74**, 1246 (1995).
[8] M. Bär, C. Zülicke, M. Eiswirth, and G. Ertl, J. Chem. Phys. **96**, 8595 (1992).
[9] J. M. Davidenko, A. M. Pertsov, R. Salomonsz, W. Baxter, and J. Jalife, Nature **353**, 349 (1991).
[10] J. Lechleiter, S. Girard, E. Peralta, and D. Clapham, Science **252**, 123 (1991).
[11] Th. Mair and S. C. Müller, J. Biol. Chem. **271**, 627 (1996).
[12] A. S. Mikhailov, *Foundations of Synergetics I* (Springer, Berlin, 1994).
[13] E. Mihaliuk, T. Sakurai, F. Chirila, and K. Showalter, Phys. Rev. E **65**, 065602(R) (2002).
[14] Th. Schmidt, S. Heun, J. Slezak, J. Diaz, K. C. Prince, G. Lilienkamp, and E. Bauer, Surf. Rev. Lett. **5**, 1287 (1998).
[15] E. Bauer, Rep. Prog. Phys. **57**, 895 (1994).
[16] A surface analysis with Auger electron spectroscopy yielded only carbon as detectable contamination.
[17] L. H. Veneklasen, Rev. Sci. Instrum. **63**, 5513 (1992).
[18] The actual dimensions might be different due to field distortions by the charged defect.
[19] H. H. Rotermund, S. Nettesheim, A. von Oertzen, and G. Ertl, Surf. Sci. **275**, L645 (1992); **331**, 322 (1994).
[20] M. Bär, N. Gottschalk, M. Eiswirth, and G. Ertl, J. Chem. Phys. **100**, 1202 (1994).
[21] D. Barkley, Physica D **49**, 61 (1991).
[22] The grid size is 512×512 with spatial resolution $\Delta x=0.25$. The integrations were performed by a simple Euler scheme with time step $\Delta t=0.01$ and a five-point Laplacian.